Structure and Mobility of Defects Formed from Collision Cascades in MgO

B. P. Uberuaga,[1] R. Smith,[1,*] A. R. Cleave,[2] F. Montalenti,[3] G. Henkelman,[1] R. W. Grimes,[2]
A. F. Voter,[1] and K. E. Sickafus[1]

[1]*Los Alamos National Laboratory, Los Alamos, New Mexico 87545, USA*
[2]*Department of Materials, Imperial College, Prince Consort Road, London SW7 2BP, United Kingdom*
[3]*INFM, L-NESS, and Dipartimento di Scienza dei Materiali, Università degli Studi di Milano-Bicocca,
Via Cozzi 53, I-20125 Milan, Italy*
(Received 12 November 2003; published 19 March 2004)

We study radiation-damage events in MgO on experimental time scales by augmenting molecular dynamics cascade simulations with temperature accelerated dynamics, molecular statics, and density functional theory. At 400 eV, vacancies and mono- and di-interstitials form, but often annihilate within milliseconds. At 2 and 5 keV, larger clusters can form and persist. While vacancies are immobile, interstitials aggregate into clusters (I_n) with surprising properties; e.g., an I_4 is immobile, but an impinging I_2 can create a metastable I_6 that diffuses on the nanosecond time scale but is stable for years.

In this Letter, we combine four computational techniques to perform multi-time-scale simulations of radiation-damage effects in solids. For the first time, we predict, without any prior assumptions about the dynamics, the fate of defects generated under ballistic radiation-damage conditions out to time scales approaching those which can be probed experimentally (i.e., order of seconds). A typical molecular dynamics (MD) simulation of radiation damage follows the evolution of an isolated collision cascade over picosecond (ps) time scales, which is sufficient to observe the collisional phase of the cascade and to identify characteristic features of the residual defects left by the cascade process (see, e.g., Ref. [1]). However, the actual behavior of a material is determined not only by the number and nature of the residual defects associated with a cascade event, but also by the long-time evolution of those defects. Over time scales much greater than ps, residual defects can both annihilate and aggregate. Annihilation events effectively promote radiation tolerance; aggregation events, on the other hand, lead to decreased probability for annihilation and consequently exacerbate radiation-damage susceptibility. In order to effectively predict radiation-damage evolution in a material, one must necessarily gain access to longer time-scale processes such as defect mobility, annihilation, and aggregation. The work presented here represents our inaugural attempt to expand radiation-damage predictive capabilities via computation. By merging conventional MD cascade simulations with accelerated dynamics methods, we can monitor the evolution of cascade debris to times of the order of milliseconds (ms) to seconds (s).

As a model material for this study, we chose the oxide magnesia (MgO). Oxides are the conventional nuclear fuel form used in light water reactors (UO_2 and mixed oxides [2]) and are attractive as insulators for fusion reactor diagnostics [3]. Also, there is growing interest in their use as host materials for the immobilization and long-term storage of toxic radionuclides such as the transuranics found in spent nuclear fuel [4,5]. MgO is a classic engineering ceramic with well-understood properties, and its radiation-damage behavior has been the subject of numerous experimental and computational investigations. Finally, well-established empirical potentials exist for MgO.

The computational procedure used here consisted of four components. As detailed below, we first generated collision cascades in MgO at selected energies using MD for a few ps. We adopted representative defect configurations from the cascades and used these as starting configurations for long-time simulations via temperature accelerated dynamics (TAD) [6,7]. We also used static energy minimization to assess the relative stability of defects observed in MD or TAD simulations against alternative crystallographic arrangements of the same defect. Finally, key findings were verified using the higher-quality description afforded by density functional theory (DFT).

Using this approach, an interesting picture emerges for the room-temperature evolution of radiation damage after a low-energy cascade in MgO. In the first 10 ps, a primary knockon atom (PKA) (the atom imparted with the collision energy from, for instance, an energetic neutron) event typically creates a small number of interstitials and vacancies. While the vacancies are essentially immobile, isolated interstitials diffuse on the nanosecond (ns) time scale. Point defects are charged, so the interstitials are quickly drawn to either a vacancy and annihilated or to another interstitial to form a neutral di-interstitial cluster, which is mobile on the ms time scale. While clusters generally become less mobile with size, we have observed a surprising nonmonotonicity. A hexa-interstitial cluster can form which diffuses much faster than the smaller clusters. This behavior impacts both the expected level of damage produced per cascade, as well as the interaction between cascades.

The potential used here, based on that given by Lewis and Catlow [8], is pairwise additive, consisting of an electrostatic part and a standard short-range Buckingham term. Shells were not included in the MD and TAD simulations but were included in some energy minimizations for comparison. The potential is a full charge model, which recent *ab initio* calculations confirm is maintained by the ions in this lattice [9]. The potential is not sufficiently repulsive for the small distances encountered during cascades and so was modified by a screened Coulomb potential [10]. We applied a smooth cutoff to the Buckingham term at distances greater than 8 Å for the O-O interactions and 5.5 Å for the Mg-O interactions. Both Ewald sums and the fast multipole method implemented by Rankin [11] were used to calculate the Coulombic interactions. This model does not account for charge transfer. Specifically, we do not account for defects such as F^+ and F centers (anion vacancies with one and two trapped electrons, respectively) in our calculations. An anion vacancy in our model is formally an F^{++} center with no trapped electrons. The same is true for cation vacancies.

Collision cascades with PKAs at energies of 0.4, 2, and 5 keV were investigated. Crystal sizes varied from 4000 to 160 000 atoms, the size chosen to ensure that the cascades did not interact strongly with the cell boundaries. Trajectories were run for up to 8 ps or until the thermal spike of the cascade had dissipated throughout the cell. Initial trajectory directions were randomly distributed over a solid angle representative of the crystal symmetry. In total, 20 trajectories were run at 0.4 keV, and 12 each at 2 and 5 keV, evenly distributed between an O and a Mg PKA. Each trajectory was begun at a temperature of $T = 0$ K. Previous MD work has indicated [12] that the displacement energy threshold in MgO is very high: about 65 eV for an O and 90 eV for a Mg PKA. We obtain similar but slightly higher values.

Figure 1 shows a typical cascade with a PKA energy of 0.4 keV. Shortly after the initial knockon, a large number of atoms are displaced from their original lattice site, peaking at $t = 80$ fs [Fig. 1(a)]. After 260 fs, most of the
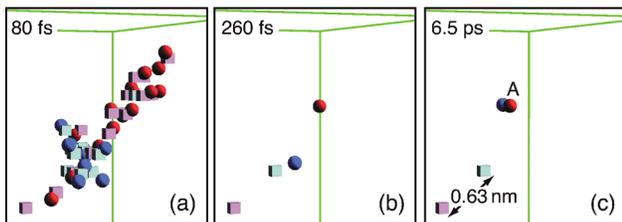

FIG. 1 (color). The defects in a cascade generated from a 0.4 keV O PKA. The scheme—used in all figures—is dark blue spheres for Mg interstitials, dark red spheres for O interstitials, light blue cubes for Mg vacancies, and light red cubes for O vacancies. (a) At $t = 80$ fs, the number of displaced atoms peaks. (b) By $t = 260$ fs, most of the defects have recombined and only a few isolated defects remain. (c) By $t = 6.5$ ps, the interstitials have formed a di-interstitial (labeled A).

damage has annealed, leaving only two vacancies and two separated interstitials [Fig. 1(b)]. However, by $t = 6.5$ ps, by which time the cascade has settled down, the two interstitials have attracted one another and formed a MgO di-interstitial [Fig. 1(c)]. In other cases, the interstitial recombined with a nearby vacancy. Whether the interstitial prefers to move toward another interstitial or toward a vacancy depends on the complex electric field created by these scattered point defects.

For 0.4 keV, only a small number of defects formed. The number of Frenkel pairs, or atoms that were still displaced after the 8 ps simulation time, was 0.5 per trajectory. These were evenly divided between interstitial-vacancy pairs separated by over 1 nm (pairs separated by less than 1 nm quickly recombined) and MgO di-interstitials. Interstitials were located at the body center of the 8-atom MgO cell, or the 8c site. The number of atoms displaced from their original lattice site was much larger, averaging nine per trajectory. Most recombined with vacancies very quickly, as shown in Figs. 1(a) and 1(b). The results of each of the cascade energies simulated are summarized in Table I.

As expected, the number of defects that survive the collisional phase of a cascade ($t = 8$ ps) increases dramatically with PKA energy. At 2 keV, seven Frenkel pairs formed per trajectory while 18 formed at an energy of 5 keV. The number of displaced atoms also rose, to 48 atoms per trajectory at 2 keV and 124 at 5 keV. The increase in the number of defects with PKA energy was accompanied by an increase in the size of interstitial clusters. At 0.4 keV, only isolated interstitials and di-interstitials were formed. Tri-interstitials began to appear at 2 keV and, at 5 keV, a number of larger clusters, including four tri-interstitials, a tetra-interstitial, and one 7-atom cluster, formed. A similar trend is seen for vacancy clusters. For all energies, the isolated interstitials were roughly evenly divided between O and Mg. Examples of defects at the end of the higher energy cascades are shown in Fig. 2.

Typical defects found in the cascade simulations were analyzed via static energy minimization using the procedure described in Ref. [13]. The binding energies ($E_{\text{isolated defects}} - E_{\text{cluster}}$), calculated without shells, for

TABLE I. The total number of Frenkel pairs (N_{FP}), principal defect types, and times the lattice reformed perfectly (N_{PL}) for PKA energies of 0.4, 2, and 5 keV remaining after the collisional phase ($t = 8$ ps) of a cascade. In addition, one tri-interstitial formed at 2 keV and four tri-interstitials, one tetra-interstitial, and one 7-interstitial cluster formed at 5 keV.

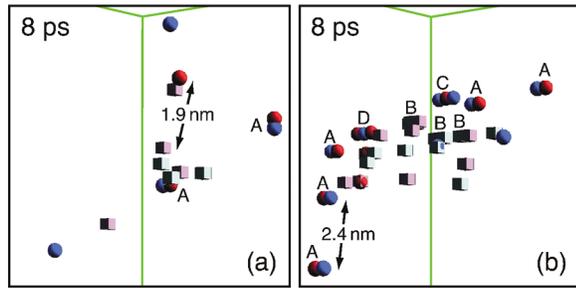| PKA energy (keV)	No. of trajs.	N_{FP}	No. of defects		di-int	di-vac	N_{PL}
			mono-int O/Mg	mono-vac O/Mg			
0.4	20	10	3/1	5/3	3	1	13
2	12	84	21/24	33/30	15	6	0
5	12	216	57/62	78/80	39	15	0

FIG. 2 (color).   (a) Typical defects remaining after the collisional phase ($t = 8$ ps) of a cascade for a PKA energy of 2 keV. Shown are several isolated vacancies and interstitials plus two di-interstitials (labeled A). (b) Residual defects 8 ps after a 5 keV PKA event. In addition to isolated vacancies, interstitials and di-interstitials (A), di-vacancies (B), and tri-interstitials of both types—Mg-O-Mg (C) and O-Mg-O (D)— form.
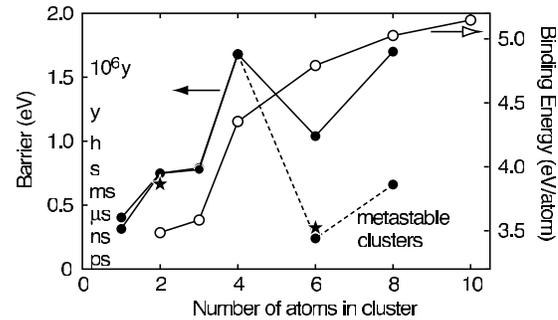

FIG. 3.   Binding energy and diffusion barriers for interstitial clusters versus cluster size. The time scale for diffusion at 300 K is also shown. The binding energy increases with the cluster size, while the energy barriers do not follow any obvious trend. The dashed line indicates barriers for metastable clusters. The ★s indicate barriers calculated with DFT.

the most stable interstitial configurations are shown in Fig. 3. The interstitial clusters exhibit strong binding energies which increase from 3.49 eV per atom for the di-interstitial to 5.15 eV per atom for the deca-interstitial cluster. The same trend occurs when shells are included, although the binding energies are about 0.7 eV smaller per atom. As suggested by the cascade simulations, isolated interstitials were found to be most stable at the 8c site. This result is in agreement with other calculations for the charged interstitial [14], although calculations on neutral interstitials find the split interstitial is more stable [15]. Static simulations were also used to identify the saddle points associated with the diffusion of the single interstitials and thus we predict the energy barriers for diffusion: 0.40 eV for O and 0.32 eV for Mg.

The cascade simulations can only follow the evolution of the resulting defects for ps. We applied TAD [6,7] to representative defects to achieve experimental time scales. TAD involves running MD at a high temperature T_{high} in a way that constrains the dynamics to the current basin. The times of attempted events seen at T_{high} are extrapolated to the temperature of interest T_{low} and the event occurring earliest at T_{low} is accepted. The process is repeated in the new state. Here, T_{low} was set to 300 K.

In MgO, the barriers for defect diffusion range from 0.25 to over 2 eV. To enhance the speed of the TAD simulations, we used a recently developed extension to TAD, the dimer-TAD method [16], which exploits the dimer method [17] to find the minimum barrier to leave a state. This barrier is used to reduce the amount of MD that must be performed at T_{high} and to tune T_{high} for each state, resulting in values between 300 and 2000 K.

In the TAD simulations, we employed systems containing 512 and 1728 atoms. A periodic cell was used to study neutral defects and a cell with free surfaces was used for the tri-interstitials. The diffusion barriers found from the TAD simulations for the key interstitial clusters are summarized in Fig. 3. At 300 K, vacancies are immobile (barrier > 2 eV) while interstitials diffuse on ns time scales. For small clusters, the diffusion barrier increases

with size: mono-interstitials diffuse quickly, di- and tri-interstitials diffuse more slowly with barriers of 0.75 eV (di-interstitial) and 0.79 eV (Mg-O-Mg) or 0.80 eV (O-Mg-O) (s time scale), and tetra-interstitials, with a barrier of 1.68 eV, are immobile (see Fig. 4). Tetra-interstitials are also very stable: the barrier to split them is 2.5 eV, a process that basically never occurs at 300 K.

This trend suggests that clusters of four or more interstitials act as immobile interstitial sinks. Surprisingly, however, the hexa-interstitial is mobile, with a diffusion barrier of 1.04 eV in its ground state (100 s time scale). Moreover, it can exist in a metastable state, a state actually formed in an encounter between a di- and a tetra-interstitial during the TAD simulation shown in Fig. 4. This state diffuses on the ns time scale with a barrier of 0.24 eV and is limited to one-dimensional diffusion along a $\langle 110 \rangle$ direction. The barrier to decay to the ground state is 1.31 eV, so a cluster formed in this metastable state will last for years.

While we have not explored it completely, we find the behavior of the octa-interstitial is similar to that of the hexa-interstitial. A metastable structure diffuses one dimensionally with a barrier of 0.66 eV, trapped by a barrier of 1.52 eV for decay to the immobile ground state. Larger clusters may have interesting properties as well.

TAD simulations also show that, as in other systems [7], activated processes often involve concerted motion of many atoms. For example, the metastable hexa-interstitial moves by a 12-atom mechanism. In addition, as interstitial and vacancy defects interact in the strong Coulomb field, long-range concerted events can lead to their annihilation over distances of many angstroms.

For convenience, all simulations were performed on systems held at the $T = 0$ K lattice constant. Expanding to the $T = 300$ K lattice constant changes the barriers slightly; e.g., the barrier for the tetra-interstitial changes from 1.68 to 1.61 eV and that for the metastable hexa-interstitial changes from 0.24 to 0.21 eV.

We have tested some of the empirical potential results with DFT, using the VASP code [18] with the PW91
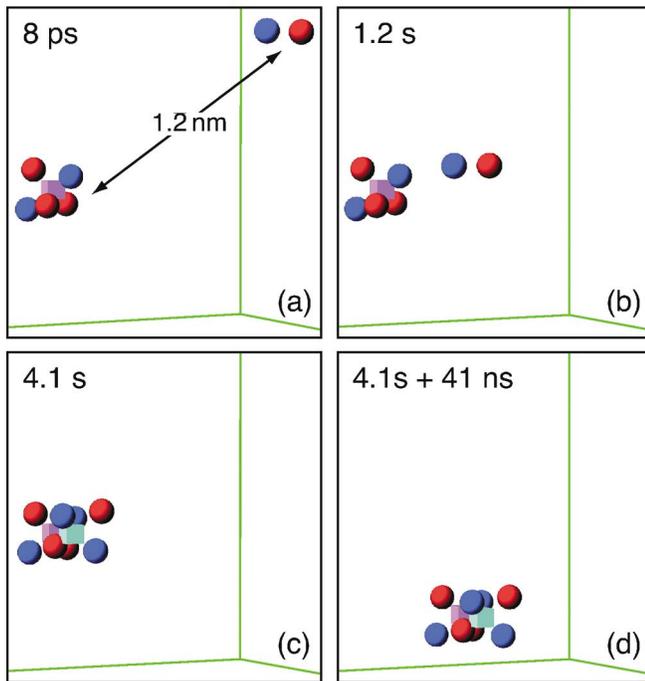
FIG. 4 (color). TAD simulation of the formation of a hexa-interstitial at 300 K. (a) A di- and a tetra-interstitial began about 1.2 nm apart. (b) By $t = 1.2$ s, the di-interstitial approached the immobile tetra-interstitial. (c) By $t = 4.1$ s, the combined cluster annealed to form the metastable hexa-interstitial, (d) which diffuses on the ns time scale with a barrier of 0.24 eV.

functional and the projector augmented wave method [19] on supercells containing 216 lattice atoms. A plane wave basis with energies up to 400 eV was used. It was determined that a single Γ-point sampling of k space was sufficient to converge energies for this cell size. We compared DFT and the empirical potential for both the formation and the migration energy of the di- and metastable hexa-interstitials. The DFT formation energies are 12.8 and 31.1 eV, respectively, which compare well with the empirical potential values of 11.9 and 28.5 eV, considering the high energies involved in the collision cascades. The diffusion barriers for both defects agree very well: 0.66 and 0.33 eV using DFT compared to the empirical potential values of 0.75 and 0.24 eV (see Fig. 3).

Combining the results from these four computational methods has led to the picture described above for the evolution of radiation damage in MgO. Point defects and small clusters form during low-energy cascades. While vacancies are immobile at room temperature, interstitials diffuse quickly, either recombining with vacancies or clustering with other interstitials. Interstitial clusters become more stable with size, but certain sizes and forms can be very mobile. They can thus aggregate with clusters from other cascades, increasing the overall damage accumulation rate. In the case of the hexa- and octa-interstitials, the long-range one-dimensional diffusion along $\langle 110 \rangle$ in the metastable state could result in an experimentally detectable signature.

In summary, combining MD cascade simulations, static energy minimization, temperature accelerated dynamics, and DFT, we find that it is possible to study the radiation-damage properties of MgO on time scales relevant to experiment. Complex events are important, and higher level models should account for them in order to simulate the correct damage evolution.

*Permanent address: Department of Mathematical Sciences, Loughborough University, LE11 3TU, Loughborough, United Kingdom.
[1] D. J. Bacon and T. D. de la Rubia, J. Nucl. Mater. **216**, 275 (1994).
[2] D. R. Olander, "Fundamental Aspects of Nuclear Reactor Fuel Elements," Technical Information Center, Office of Public Affairs, Energy Research and Development Administration, Springfield, Virginia, 1976.
[3] C. Kinoshita and S. J. Zinkle, J. Nucl. Mater. **233–237**, 100 (1996).
[4] S. X. Wang et al., J. Mater. Res. **14**, 4470 (1999).
[5] K. E. Sickafus et al., Science **289**, 748 (2000).
[6] M. R. Sørensen and A. F. Voter, J. Chem. Phys. **112**, 9599 (2000).
[7] A. F. Voter, F. Montalenti, and T. C. Germann, Annu. Rev. Mater. Res. **32**, 321 (2002).
[8] G. V. Lewis and C. R. A. Catlow, J. Phys. C **18**, 1149 (1985).
[9] K. Doll, M. Dolg, and H. Stoll, Phys. Rev. B **54**, 13 529 (1996).
[10] J. F. Ziegler, J. P. Biersack, and U. Littmark, *The Stopping and Range of Ions in Solids* (Pergamon, New York, 1985), Vol. 1.
[11] W. T. Rankin and J. A. Board, Jr., in *Proceedings of the 1995 IEEE Symposium on High Performance Distributed Computing* (IEEE Comput. Soc. Press, Los Alamitos, CA, 1995), p. 17.
[12] B. Park, W. J. Weber, and L. R. Corrales, Nucl. Instrum. Methods Phys. Res., Sect. B **166–167**, 357 (2000).
[13] G. Busker et al., Nucl. Instrum. Methods Phys. Res., Sect. B **171**, 528 (2000).
[14] T. Sonoda, C. Kinoshita, and Y. Isobe, Ann. Phys. (Paris) **20**, C3-33 (1995).
[15] E. A. Kotomin et al., Defect Diffus. Forum **143–147**, 1231 (1997).
[16] F. Montalenti, B. P. Uberuaga, G. Henkelman, and A. F. Voter (to be published).
[17] G. Henkelman and H. Jónsson, J. Chem. Phys. **111**, 7010 (1999).
[18] G. Kresse and J. Hafner, Phys. Rev. B **47**, 558 (1993); **49**, 14 251 (1994); G. Kresse and J. Furthmüller, Comput. Mater. Sci. **6**, 15 (1996); Phys. Rev. B **54**, 11 169 (1996).
[19] G. Kresse and J. Joubert, Phys. Rev. B **59**, 1758 (1999); P. E. Blöchl, Phys. Rev. B **50**, 17 953 (1994).